



Deliverable 6.1

First delivery of input and validation data on electrochemical testing of components and cells

Project acronym: ECO2LIB
Project title: Ecologically and Economically viable Production and Recycling of Lithium-Ion Batteries
Grant Agreement number: 875514
Coordinator: Martin Krebs

This project has received funding from the European Union's Horizon 2020 research and innovation programme under grant agreement No 875514.

Disclaimer excluding Agency responsibility:

The information and views set out in this deliverable are those of the authors and do not necessarily reflect the official opinion of the European Union. Neither the European Union institutions and bodies nor any person acting on their behalf may be held responsible for the use which may be made of the information contained therein.

Funding Scheme: H2020-LC-BAT-2019-2020 / LC-BAT-2-2019

Delivery Date from Annex I:	December 31 st 2021
Start date of the project:	January 1 st 2020
Project duration:	54 months

Work package:	6
Lead beneficiary for this deliverable:	UW
Authors:	Maciej Ratynski, Bartosz Hamankiewicz, Andrzej Czerwinski

Dissemination level		
PU	Public	X
CO	Confidential, only for members of the consortium (including the Commission Services)	
CI	Classified	

1. BASIC ELECTRODE PARAMETERS

At 100% SoC

Table 1: Basic electrode parameters at 100% SoC.

Stoichiometry 100%	[mg]	%	concentration of Li [mol/cm ³] without volume change	concentration of Li [mol/cm ³] with volume change included	Density [g/cm ³]	Density at 100% SoC [g/cm ³]	Molecular Weight [g/mol]
Si	0.7025	19.68			2.3200	1.1-1.2*	28.08
Graphite	1.8265	51.17			2.2600	2.34	12.01 (72.06 per C6 unit)
Carbon	0.0843	2.36			2.0000	-	12.01
Binder	0.1967	5.51			1.4100	-	
Lithium in Graphite	0.1612	4.52	0.0285	0.0271	-	-	79 (g/mol Li)
Lithium in Si	0.5985	16.77	0.2823	0.0941		-	16.3 (g/mol Li)
All Lithium	0.7597	21.28					6.94
Electrolyte			0.00100			1.454	LiPF ₆ : 151.9

* (Kim, Chou, Ekerdt, & Hwang, 2011)

The stoichiometry at 0% SoC (with lithium) is very hard to estimate due to the very low Lithium (Li) content. The approximation was, that at 0% SoC, the electrode composition is equal to pristine electrode composition.

The maximum Li concentration at graphite and Silicon with 5% and 300% volume gain respectively was:

- Graphite 0.0298 mol/cm³
- Silicon 0.1036 mol/cm³

The average (by weight) was 0.0503 mol/cm³ for all active materials.

2. PHYSICAL PARAMETERS – GEN 1

Material composition

The weight composition of the Generation 1 electrodes was provided by VARTA Innovation. The electrode layer was received in February 2021. The volume composition was calculated based on the pure material density.

Table 2: Composition of the Generation 1 electrode materials.

Material	Weight %	Density* [g/cm ³]	Volume %	Volume including pores %	Reference
Elkem Silicon	25	2.32	23.4	18.2	(Greenwood & Earnshaw, 1997)
BTR918 Graphite	65	2.26	62.5	48.6	
LiPAA 450k	7	1.41	10.8	8.4	http://polymerdatabase.com/polymer%20physics/Polymer%20Density.html
Super P carbon	3	2.0	3.3	2.5	(Schwan, Ulrich, Theel, Roth, & Ehrhardt, 1997) (McCulloch, McKenzie, & Goringe, 2000) (Masaya, 2002)
Pores	-	-	0	22.3	calculated

Layer thickness and porosity

Three sets of electrodes were prepared by using different calendaring pressures resulting in different layer thickness and porosity. The porosity was calculated based on the electrode materials total volume divided by the measured electrode volume.

Table 3: Generation 1 electrode layer thickness and porosity.

Pressure [kg/cm ²]	Electrode thickness [μm]	Porosity %	Copper thickness [μm]
<10	34.5 ±0.7	41	9.7 ±0.7
2000	26.1 ±1.1	22	-
9000	20.6 ±0.8	2	-

The electrode thickness was measured by a Max-control MC-CT200 layer-meter using the magnetic field measurement mode. A plastic calibration plate was placed on the top of the electrode to avoid crushing of the active layer by the measuring probe tip.

Electrodes dimensions and masses

All electrodes were cut by an EI-cell electrode cutter with a theoretical diameter of 9 mm. The real diameter was found to be slightly lower at 8.98 ±0.04 mm.

The electrode masses were tested on a 0.01 mg balance. The average of 19 samples is presented in Table 4.

Table 4: Generation 1 electrode dimensions and masses.

	Per electrode [mg]	Per cm ² [mg/cm ²]
Whole electrode	8.55± 0.09	13.44± 0.15
Active layer	2.81± 0.09	4.41± 0.15
Silicon + graphite	2.53± 0.09	3.97± 0.13
Copper collector	5.74± 0.02	9.03± 0.04

The geometrical surface area of each electrode was 0.633 cm². The electrochemical surface area (ECSA) was roughly calculated using the equation 1 from (Ratynski, et al., 2020). The value of radius and volume used for the calculation is presented in the Material properties section. The final ECSA of the Gen 1 electrode is 20.8 cm² per electrode or 32.86 cm² per geometrical cm².

The 20.8 cm² electrode surface area value was used in all electrochemical calculations.

3. ELECTRICAL CONDUCTIVITY – GEN 1

The current collector conductivity is so high it cannot be directly measured on our system. We thus assumed that the copper conductivity is equal to theoretical value. The resistance of 1 cm² of current collector across its thickness is then equal to 1.65e-9 Ohms.

However, the copper oxides may be formed at the copper surface, especially during elevated temperatures (oven drying etc.)¹. Based on the reported data, we predicted the worst-case scenario in which the oxide thickness is 100 nm (it is very unlikely to happen, normally less than 10nm of oxide is present). In this case, the resistance of the current collector across its

¹ (Roy & Wright, 1996)

thickness is 0.2 mOhm. This value is at least 5 orders of magnitude lower than the resistance of the active layer and thus can be neglected.

The electrodes and active material resistivities were measured using a 4-point system. The electrodes and silicon were tested at two different pressures: 1.5 and 3 tons/cm².

Table 5: Generation 1 electrode and active material resistivities.

Electrode resistivity (ohm*m)		
	average	Std deviation
1.5t	148.64	6.82
3.0t	92.71	6.74

Elkem powder resistivity (Ohm*m)		
	average	Std deviation
1.5t	9,092.33	371.93
3.0t	2,807.27	117.96

BTR powder resistivity (Ohm*m)		
	average	Std deviation
2.25t	3.60	0.32

According to (Pearson & Bardeen, 1949), the theoretical Si conductivity at room temperature is approx. 3,000 Ohm/m. The obtained value (at 100 bar) is in good agreement with the previously reported values. The graphite conductivity was so high, only 2.25 t/cm² sample were measured. A higher compression resulted in a resistivity below the detection limit of our equipment.

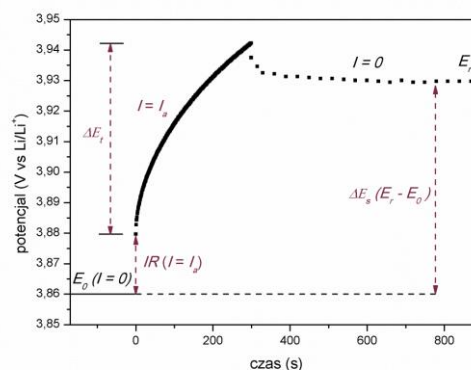
4. DIFFUSION COEFFICIENT IN ACTIVE MATERIAL – GEN 1

The parameter was measured by two techniques – GITT and EIS (Electrochemical Impedance Spectroscopy) in a 3-electrode system (Ref and Ce = Lithium metal). The GITT was performed on 4 identical cells using 1,000s pulse (C/10) and 2h OCV stabilisation time after each pulse. Ca. 40 pulses were applied at each step (charge or discharge).

The voltage profile was maintaining a linear relation to the square root from time in a range from 4s to 180-220s of the impulse. The slope of that relation was used for D calculation via the equation showed below.

Equation 1: Equation used for the diffusion coefficient calculations based on the GITT technique^{2,3}.

$$D = \frac{4}{\pi} \left(\frac{n_m V_m}{S} \right)^2 \left(\frac{\Delta E_s}{\tau \left(\frac{dE}{d\sqrt{t}} \right)} \right)^2 \quad \left(\tau \ll \frac{L^2}{D} \right).$$



² (Nysted, 2020)

³ (Nickol, et al., 2020)

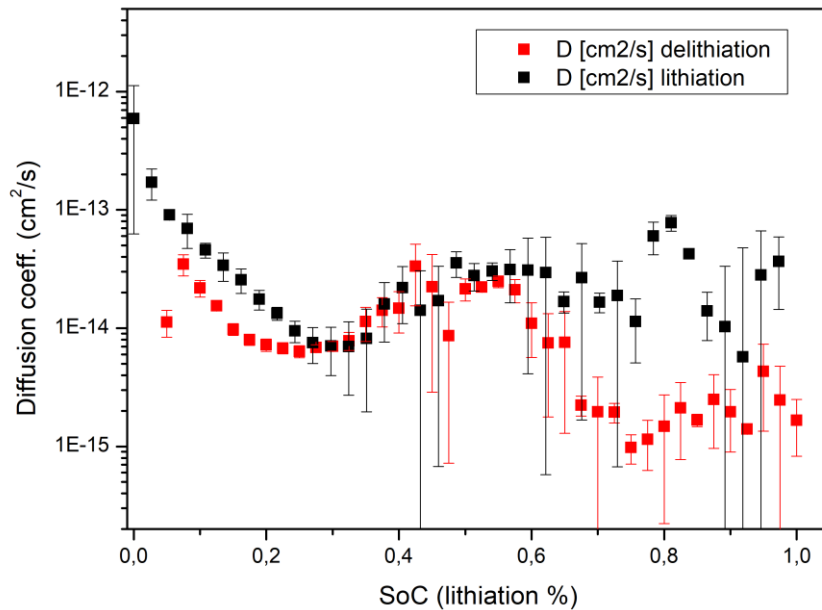


Figure 1: Diffusion coefficient obtained by GITT method.

The EIS measurement was performed 20-30 times at each step (charge or discharge).

The average of 5 cells was used for determination. Each Z'' over Z' curve was analysed in a 2Hz-0.01Hz frequency range. The part of the low frequency impedance having the slope of 45 ± 5 degrees was qualified for the D determination. The $[Z]$ over square root of angular frequency slope was extracted from the data, and the D was calculated using that slope.

Similar to the GITT results, the D value has a hysteresis loop at high lithiation range. It is probably related to the different signs of internal pressure during the charge and discharge process. The same behaviour is visible also for low lithiation degree. The D value increased over 10 times. Similar results were obtained in SINTBAT project. The D increase is probably related to the formation of “the dense phase” of silicon. Apparently, the D value from EIS is generally 1 order of magnitude lower than the value from GITT.

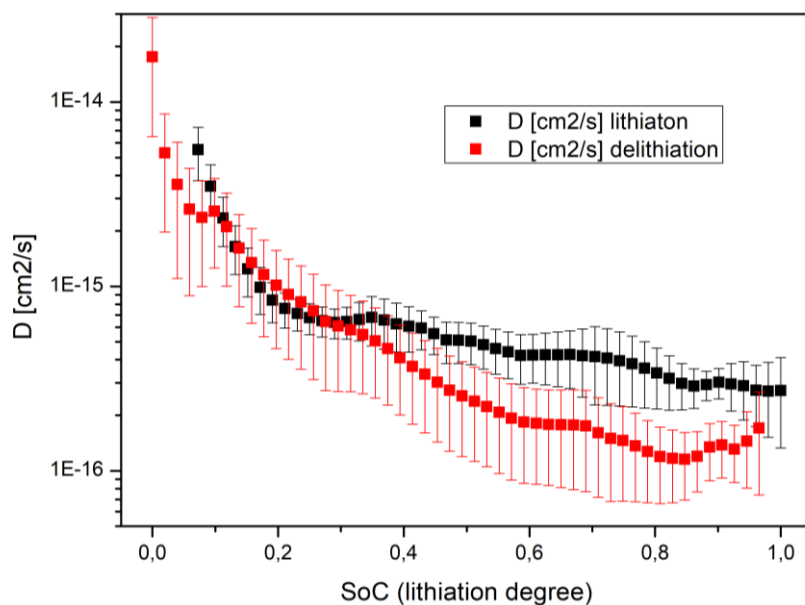


Figure 2: Diffusion coefficient obtained by EIS method.

5. CHARGE TRANSFER AND SEI LAYER RESISTANCE - GEN 1

All measurements were done in a 3-electrode cell (Li metal as CE and REF). 5 identical cells were assembled. 1Mhz- 0,01Hz data was recorded at 7 mV AC amplitude. The data was fitted in a RelaxIS 3 software by the Randles circuit:

I-R-(R)(CPE)-(R)(CPE)-(CPE)

The presence of inductance is related to cable and cell inductance. Typically, its value was in a range of $1e-7$ to $1e-8$ Henr.

The last CPE is related to the diffusion of Li^+ in the solid material. The CPE was used instead of the Warburg element because it was shown to produce more accurate results for imposed RCT/RSEI semicircle parameters. Since the slope of the diffusion was not always 45 degrees, the Wo should be used; however, the very narrow frequency range for pure diffusion (without capacitance limitations) lead to big errors in Wo parameters and corresponding big errors of the RCT value. All data are for the 0.636 cm^2 electrode (9mm diameter).

The SEI resistance was ca. 15 ohms and was stable for most of the SoC range. An increase to 25-30 ohms was observed over 90% lithiation due to a fresh layer formation at the Si surface. A decrease to 10 ohms was visible at $SoC < 10\%$ due to probable layer cracking caused by Si shrinking (no new SEI was formed due to high potential).

The hysteresis at low SoC is related to the history of the cells. Each cell was at zero current conditions for over 24 hours before the EIS test leading to the formation of the SEI at previously cracked film (even at high potential the SEI was slowly generated).

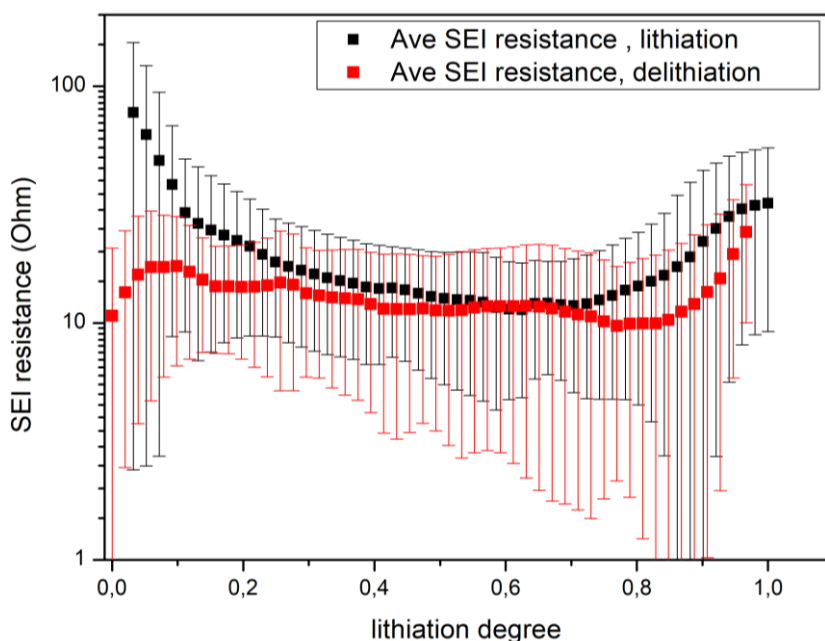


Figure 3: SEI layer resistance per electrode.

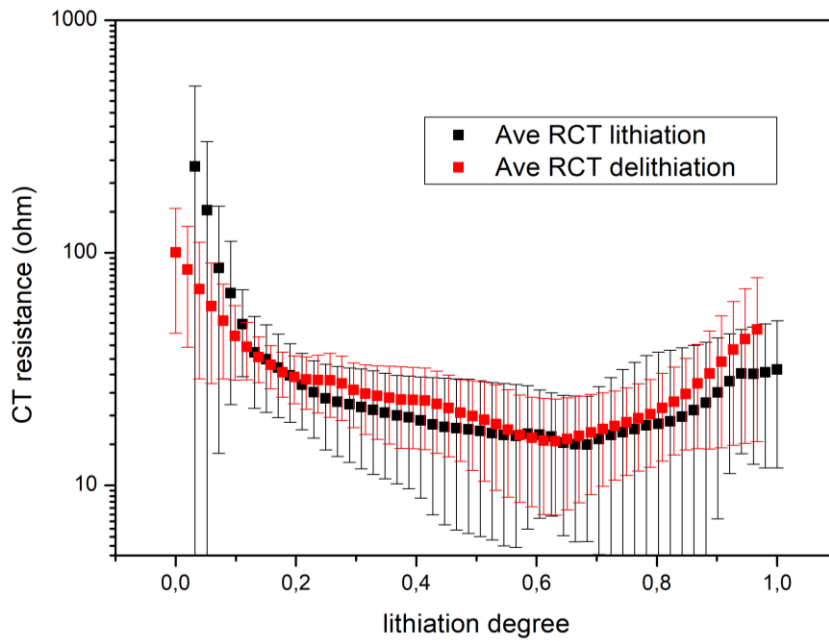


Figure 4: Charge transfer resistance per electrode

The RCT showed no hysteresis. At low SoC, the value of CT increased due to limited compression between the active material grains (low electrical conductivity). At higher SoC, the RCT increased due to Si swelling and resulting porosity decrease (bad electrolyte access and corresponding lower ECSA). The middle SoC value of RCT was close to 20 ohms.

6. PRISTINE MATERIAL PROPERTIES – GEN 1

Particle radius and surface area

The particle radius was estimated by a Laser Particle Size Analyzer (Betttersizer S3). The size of the individual grains was estimated using the Mie theory for Laser scattering analysis. The material powders were dispersed in ethanol for analysis.

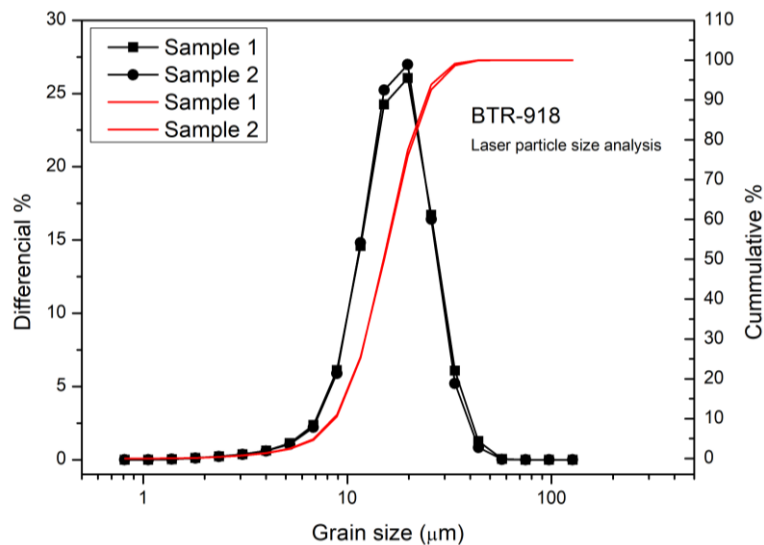


Figure 5: BTR-918 laser particle size analysis.

The average BTR-918 graphite particle diameter was 18.44 μm . The most (95%) of the particles have a size between 7 and 34 μm .

The average Elkem silicon particle diameter was 3.16 μm . The most (95%) of the particles have a size between 0.7 and 7 μm . The silicon size distribution present less Gaussian relation. Significant number of small particles below 1 micron were detected.

Both materials presented good dispersion in ethanol. No sign of agglomeration is visible.

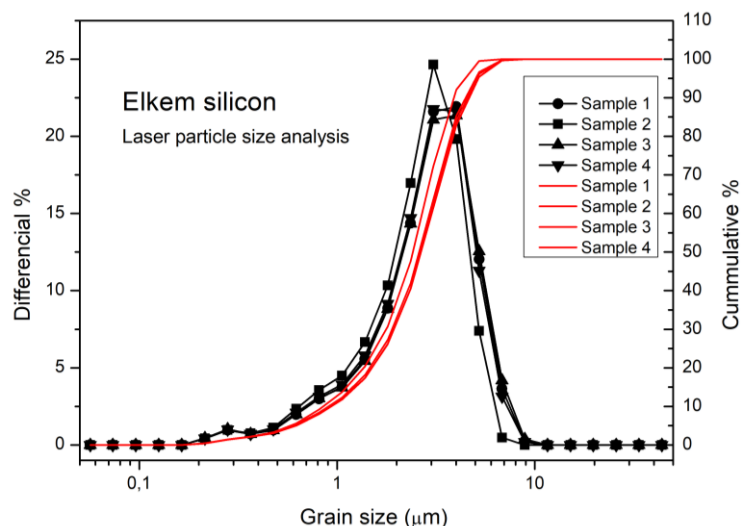


Figure 6: Elkem silicon laser particle size analysis.

BET analysis was used for the specific surface area determination, as well as for rough calculation of the particle radius. The analysis was done on the Micrometrics ASPA 2060 device by N₂ adsorption.

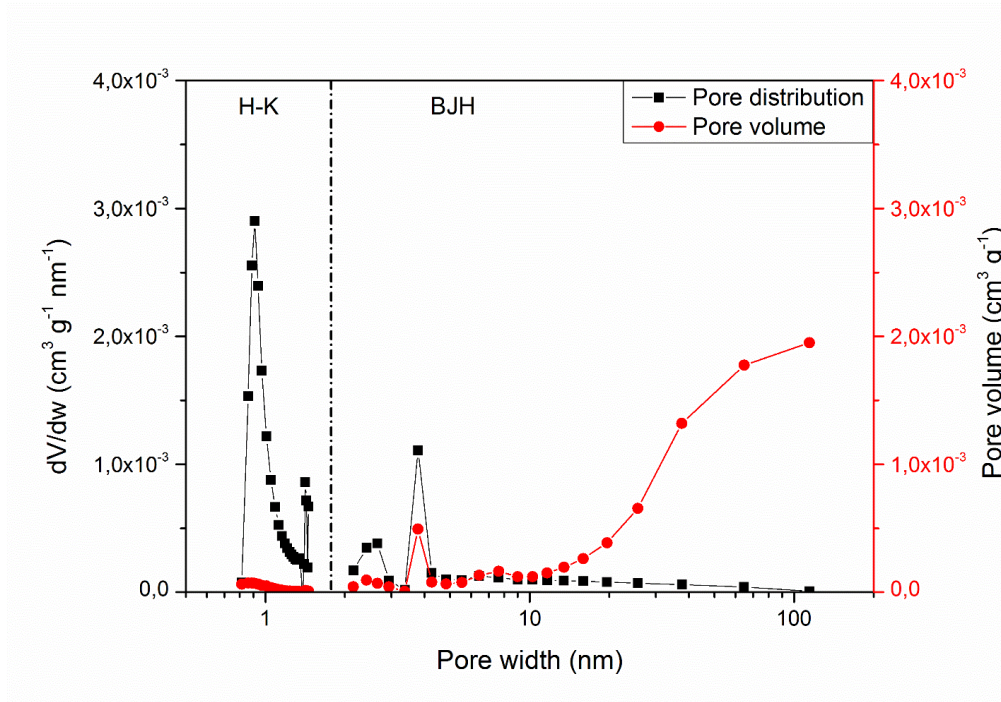


Figure 7: BTR918 BET pore distribution.

The pore distribution for BTR918 showed that the majority of the pores at the graphite surface were close to 1 nm. Such small pores are probably clogged by the SEI layer during the material operation in the cell. Slightly larger pores with a size of ca. 4 nm can be still open during material operation, leading to additional electrolyte/electrode contact surface area.

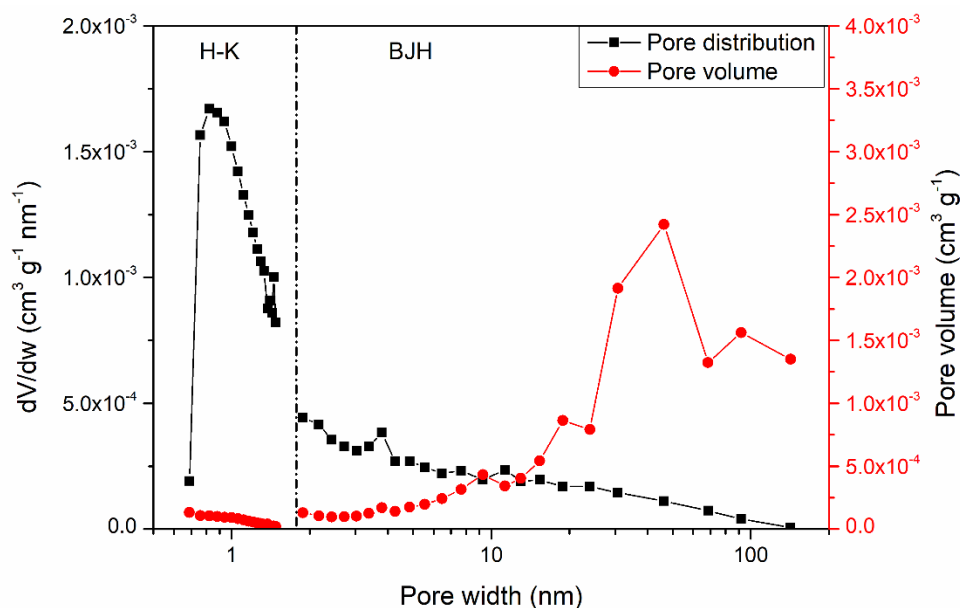


Figure 8: Elkem Si BET pore distribution.

Table 6: Elkem Si BET pore distribution.

	Area BET [$\text{m}^2 \cdot \text{g}^{-1}$]	Micropore area [$\text{m}^2 \cdot \text{g}^{-1}$]	Dominant pores [nm]	Pore volume (1.7 – 300 nm) [$\text{cm}^3 \cdot \text{g}^{-1}$]	Pore volume (<1.7 nm) [$\text{cm}^3 \cdot \text{g}^{-1}$]	Grain size [nm]
e-Si	4.71 ± 0.05	0.7	0.7-0.9; meso + macro	0.0138	0.0012	547

Table 7: Grain size and pore distribution.

	LPSA grain size [μm]	95% size range [μm]	BET surface area [m^2/g]	Main pores [nm]
BTR918	18.44	7-34	1.98	2-4
e-Silicon	3.16	0.7-7	4.71	1
Super P	0.04*	-	60.7	2-3

* (Latifatu, et al., 2018)

The average particle radius (weighted average over number of particles) was calculated as 3.36 μm . This value was used in further electrochemical calculations, when needed.

Table 8: Other important parameters of the material and electrode.

	Graphite	Silicon	Electrode	Average	Total no.
Total Volume [cm^3]	0.000808	0.000303	0,00166	-	-
Grain volume [μm^3]	3,285.7	16.513	-	19.89	-
Grain number per electrode	245,971	18,336,824		-	18,582,796
Density at 0 lithiation [g/cm^3]	2.26	2.32			
Volume change at 100% lithiation	1.05	3.0	-	-	-

Material composition

The weight composition of the Generation 1 electrodes was provided by VARTA Innovation. The electrode layer was received in February 2021. The volume composition was calculated based on the pure material density.

Table 9: Composition of the Generation 1 electrode materials.

Material	Weight %	Density* [g/cm ³]	Volume %	Volume including pores %	Reference
Elkem Silicon	25	2.32	23.4	18.2	(Greenwood & Earnshaw, 1997)
BTR918 Graphite	65	2.26	62.5	48.6	
LiPAA 450k	7	1.41	10.8	8.4	http://polymerdatabase.com/polymer%20physics/Polymer%20Density.html
Super P carbon	3	2.0	3.3	2.5	(Schwan, Ulrich, Theel, Roth, & Ehrhardt, 1997) (McCulloch, McKenzie, & Goringe, 2000) (Masaya, 2002)
Pores	-	-	0	22.3	calculated

Layer porosity (calculated)

Three sets of electrodes were prepared using different calendaring pressures resulting in different layer thickness and porosity. The porosity was calculated based on the electrode materials total volume divided by the measured electrode volume.

Table 10: Generation 1 layer porosity.

Pressure [kg/cm ²]	Porosity %
<10	41
2000	22
9000	2

7. ELECTROLYTE CONDUCTIVITY AND DIFFUSION COEFFICIENT

Conductivity

The conductivity of the FEC/EMC 3:7 1M LiPF₆ electrolyte was reported to be close to 8.9 mS/cm,⁴ which is lower than a standard EC/EMC based electrolyte or LP30 electrolyte (10.1 mS/cm @ 20°C)⁵ due to higher viscosity of the FEC and probably stronger interaction between negatively polarized fluorine group and lithium cation.

We prepared the 1M LiPF₆ in FEC/EMC 3:7 + 2%VC electrolyte from substrates provided by BASF. All tests were done using a temperature-controlled chamber and the Elmetron CX-401 conductometer with integrated temperature probe.

⁴ (Xia, et al., 2017)

⁵ (Iermakova, Dugas, Palacín, & Ponrouch, 2015)

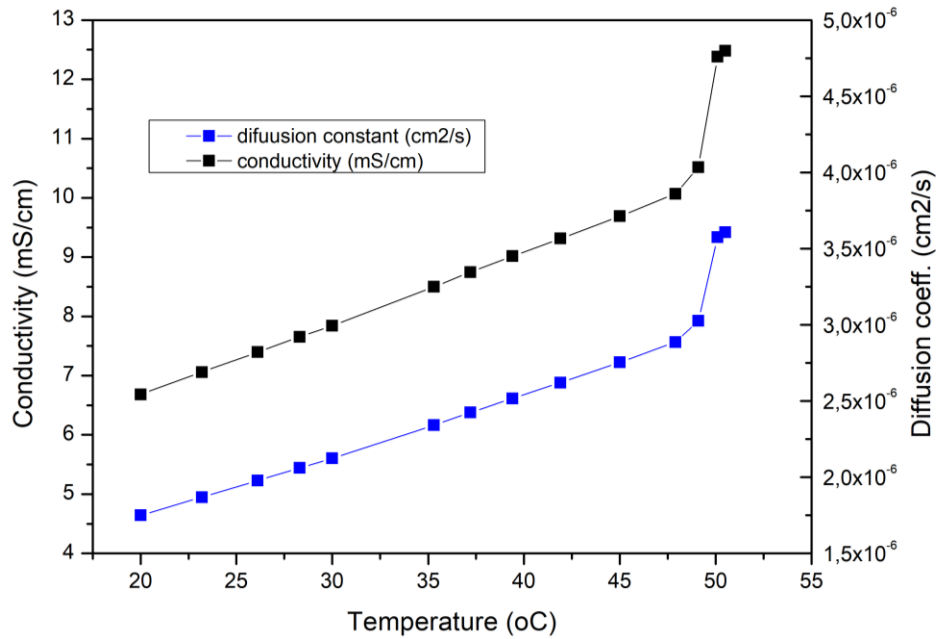


Figure 9: ECO2LIB electrolyte conductivity at different temperatures.

The diffusion coefficient was calculated using the Nernst-Einstein relation⁶. The sharp increase in the electrolyte conductivity above 50°C is probably related to the electrolyte component decomposition or the undesired reactions with the probe material.

The conductivity of the LP30 standard electrolyte was also measured. No decomposition up to 55°C was recorded. The conductivity at 20°C was 9.9 mS/cm and was in good agreement with the previously reported data.

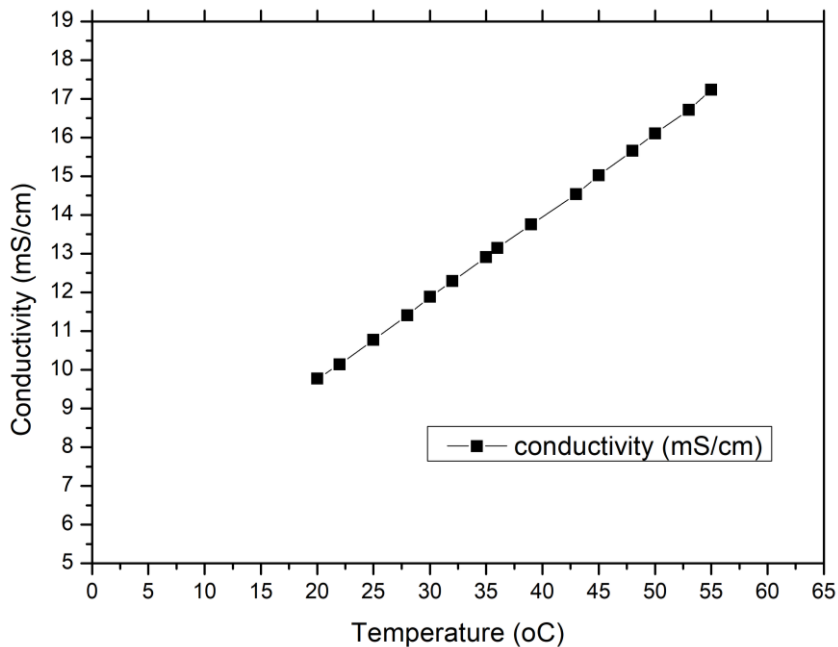


Figure 10: LP30 electrolyte conductivity at different temperatures.

⁶ (France-Lanord & Grossman, 2019)

The diffusion coefficient was also directly measured by electrochemical techniques. The determination from CV failed due to a massive lithium dendrite formation and further cell short circuit.

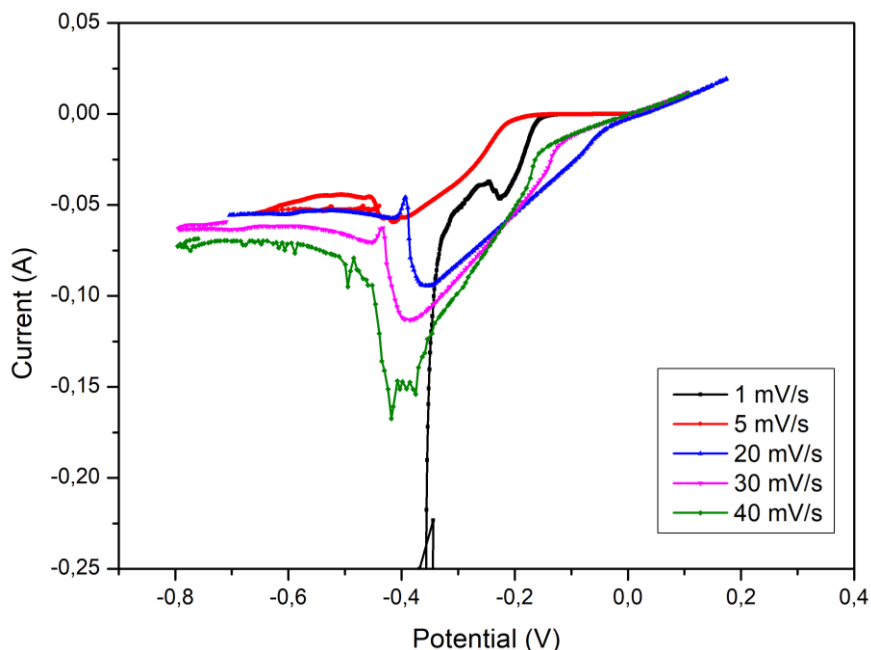


Figure 11: Cyclic voltammetry data obtained for Li-Li symmetric cell with ECO2LIB electrolyte.

The peaks were also highly moved to negative potential values due to electrode polarisation at high sweep speeds. Lower sweep rate was not possible due to dendrite formation (larger absolute charge flow) and insufficient speed of the diffusion layer formation (high diffusion constant resulted in fast mass flow). The CV results give a rational value of diffusion constant (ca. $5 \times 10^{-6} \text{ cm}^2/\text{s}$); however, the shape of the peaks was really bad and the peak high vs sweep rate^{1/2} was not passing through the zero-zero point.



Figure 12: Inside of the cell after the CV measurement. Black mass at the current collectors is the lithium dendrite structure.

Other standard electrochemical techniques such as Sand's relation for chronopotentiometry measurement⁷ also failed due to the same reasons. We determined the Diffusion parameter

⁷ (Keech, Chartrand, & Bunce, 2002)

by the galvanostatic pulse polarization experiment with long OCP stabilisation⁸. The pulse current was changed from 100 to 350 μA (per 0.81 cm^2 electrode). The pulse length was set at 720 sec. for all measurement. The OCP measurement was conducted for 7200 sec. The Li-Li distance was set to 1.33 mm. No separators were used (no need for porosity correction).

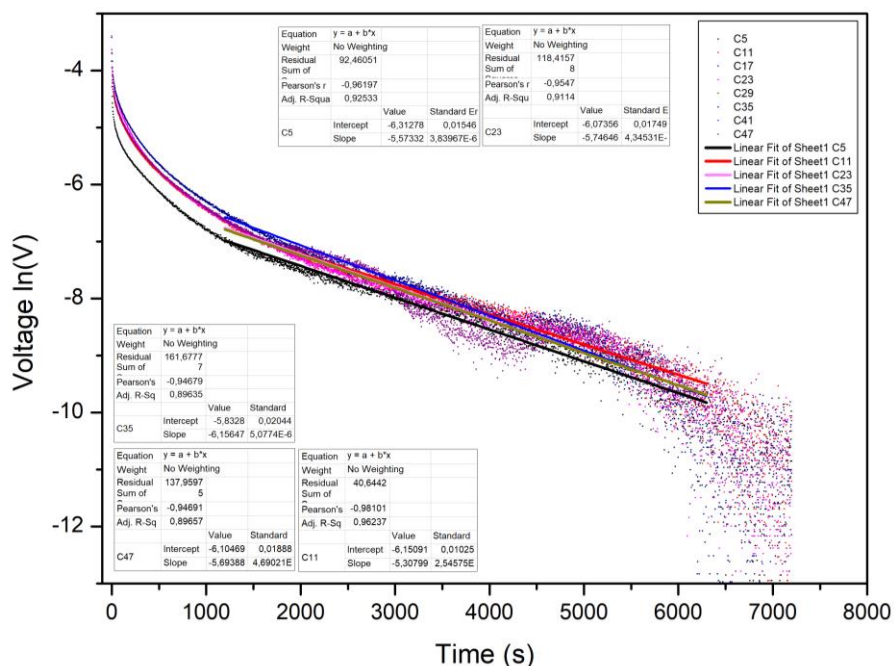


Figure 13: Voltage data recorded during OCP stabilisation experiment.

The linear voltage stabilisation was visible in 5 of 6 data sets. The difference in one sample was attributed to a temperature change of convection electrolyte mixing.

The lack of dependence of the OCP vs time plots from the peak current density is in good agreement with the theoretical assumption used for this measurement.

A standard Swagelok case was found to be impractical for this kind of measurement due to the large volume filled with electrolyte above the actual electrodes leading to nonlinear diffusion towards working electrode.

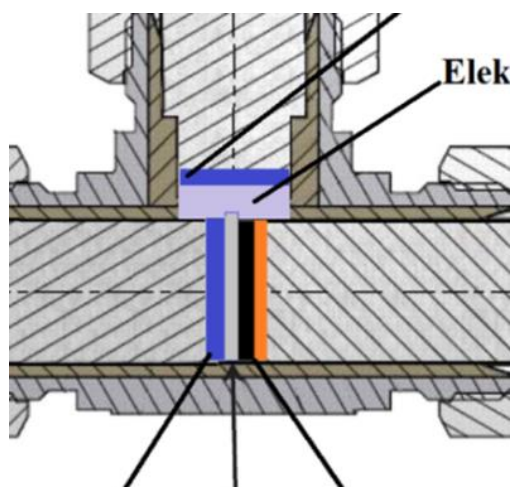


Figure 14: Scheme of the standard Swagelok measuring cell.

⁸ (Ehrl, Landesfeind, Wall, & Gasteiger, 2017)

We constructed the modified case with an almost negligible volume above the electrodes.

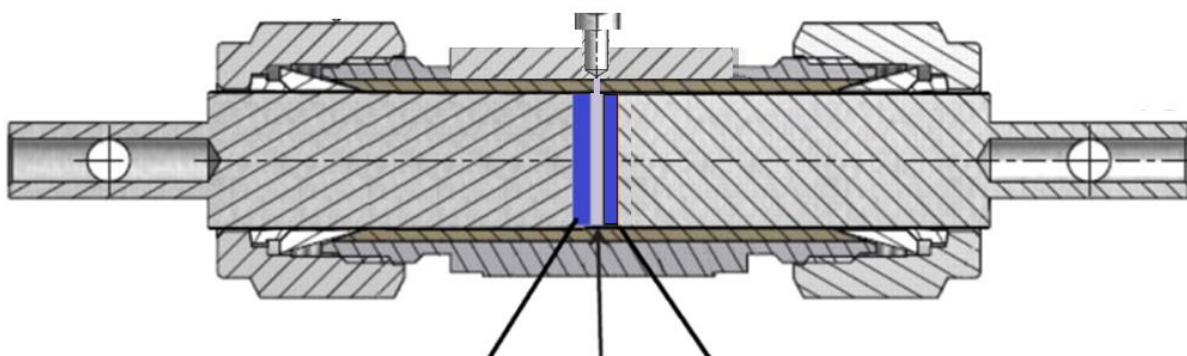


Figure 15: Scheme of the modified cell.

After this modification, we were able to determinate the diffusion coefficient of the ECO2LIB electrolyte to be:

$$D=1.02\pm 0.06 \cdot 10^{(-6)} \text{ cm}^2/\text{s}.$$

The value is in good agreement with the calculated coefficient (Nernst-Einstein equation) equal to $1.8 \cdot 10^{-6}$ at room temperature.

8. PRELIMINARY VALIDATION OF ELECTROCHEMICAL PERFORMANCE – GEN 1

Table 11: Comparison of theoretical and measured capacity.

	Ah/g	Ah/cm ²	1 st cycle efficiency %
Theoretical capacity/efficiency	1.265	5.057	>85
Measured capacity (2% porosity electrodes) (1 st delithiation @ C/20)	0.94 ± 0.21	3.76 ± 0.84	90.3
Measured capacity (22% porosity electrodes) (1 st delithiation @ C/20)	1.016 ± 0.007	4.06 ± 0.03	91.3

OCV before formation was measured after 12-24 hours cell stabilisation @ $24\pm 1^\circ\text{C}$. The measured value is 2.986 ± 0.079 V vs. Li. The Swagelok type cell contains stainless steel rods as current collectors. The effect of those rods was found to be neglectable. The OCV measuring cell containing a lithium metal stripe and ca. 5 cm^2 of Gen 1 layer was constructed using HDPE vial (ca. 20 ml) inside a glovebox (O_2 and $\text{H}_2\text{O} < 0.5 \text{ ppm}$). The OCV measurement was conducted at room temperature for 24 hours. The OCV value raised to 3.127 V during the first hour and then slowly dropped to 3.063 after 4 hours and further to 2.851 V vs. Li after 24 hours. The slightly lower OCV compared to cell measurements was probably related to electrolyte evaporation during the process (the vial was not fully sealed).

Cycling of the electrodes calendared to 2% porosity revealed a fast capacity drop.

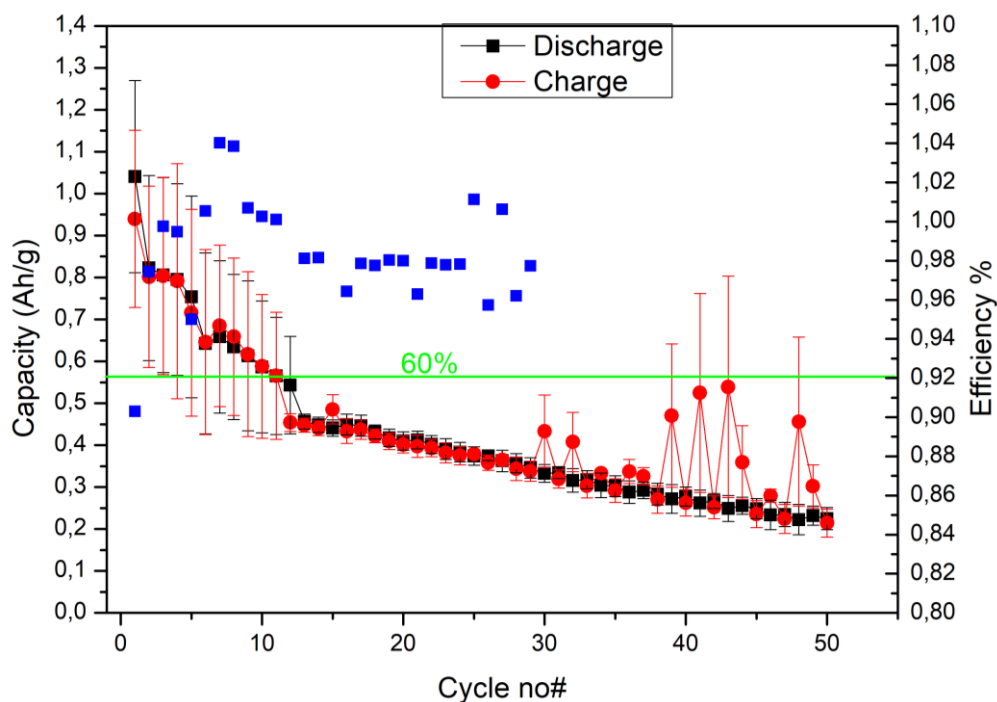


Figure 16: Specific capacity of the Gen-1 electrodes cycled at 100% DoD.

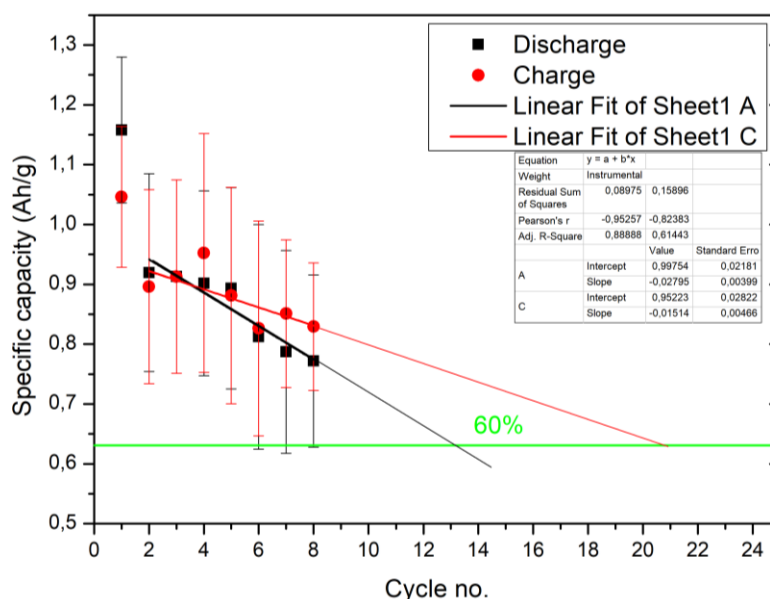


Figure 17: Best results obtained for 100% DoD cycling of Gen-1 electrodes.

Even for the best samples, the capacity fade was rapid. The estimated capacity dropped to 60% after 14-20 cycles. The cycling was performed @C/5 current. The large absolute charge passed through the cell leading to massive lithium dendrite growth on the counter electrode surface (Li metal), and finally leading to sudden death by short circuit of ca. 50% of the cell during the first 10 cycles. The post-mortem analysis of the electrodes revealed delamination from the current collector due to internal stress generation by the Si swelling.



Figure 18: Image of the Gen-1 electrodes after 50 cycles at 100% DoD.

We also noted that one of the reasons for the poor capacity retention may be insufficient lithiation due to larger resistance of the constantly growing SEI layer. Further experiments were performed using CCCV procedure at lithiation and CC at delithiation.

Electrodes with 22% porosity were used for the C-rate characteristics determination. The measurement was done using the CCCV procedure to 20 mV vs Li. The CV was held for 4 hours. Charging was done by the CC procedure. 3 identical cells were analysed.

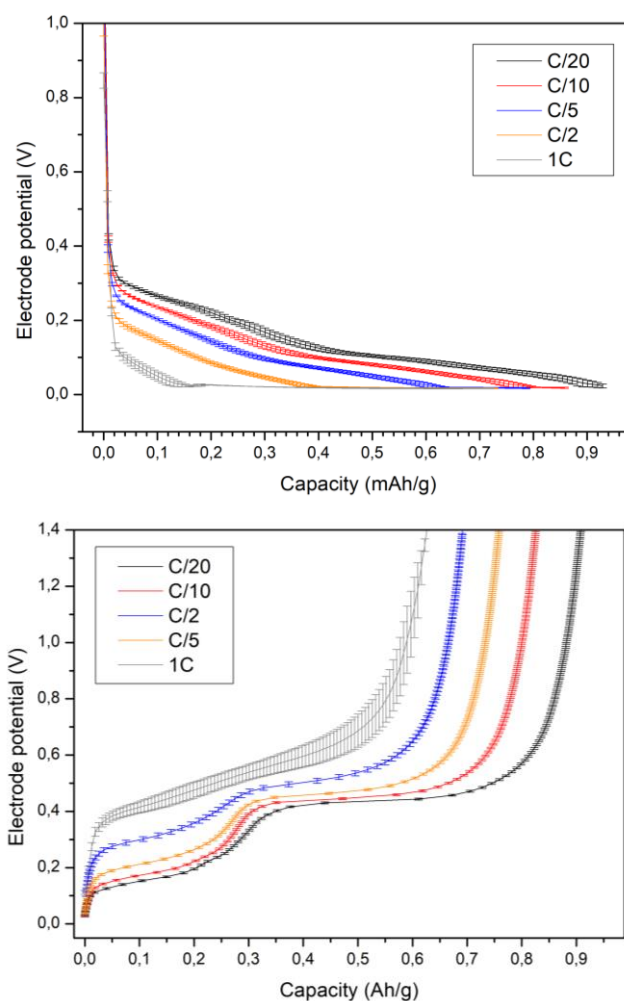


Figure 19. Lithiation and delithiation potential profiles for Gen 1 electrodes.

During the discharge, graphite and silicon were lithiated in a similar voltage range and it was not possible to distinguish the reaction. During charging, the graphite was delithiated at much lower potential compared to silicon, leading to the formation of two well visible plateaus at C/20-C/2. At 1C the plateaus disappeared due to large electrode polarisation. The same plots against electrode area were calculated (see folder).

The 22% porosity electrodes presented much better capacity retention; however, after 25 cycles only 55% of the initial capacity remained. Three identical cells were analysed (CCCV procedure), 0.02V-1.4V vs. Li at C/10.

A lower C-rate should be beneficial for the cycle life. It clearly reduced the Li dendrite formation on the counter electrode and thus resulted in low internal short circuit rate.

The CV charge increased gradually during cycling due to an increase of the internal electrode resistance and decrease in capacity (higher effective C-rate).

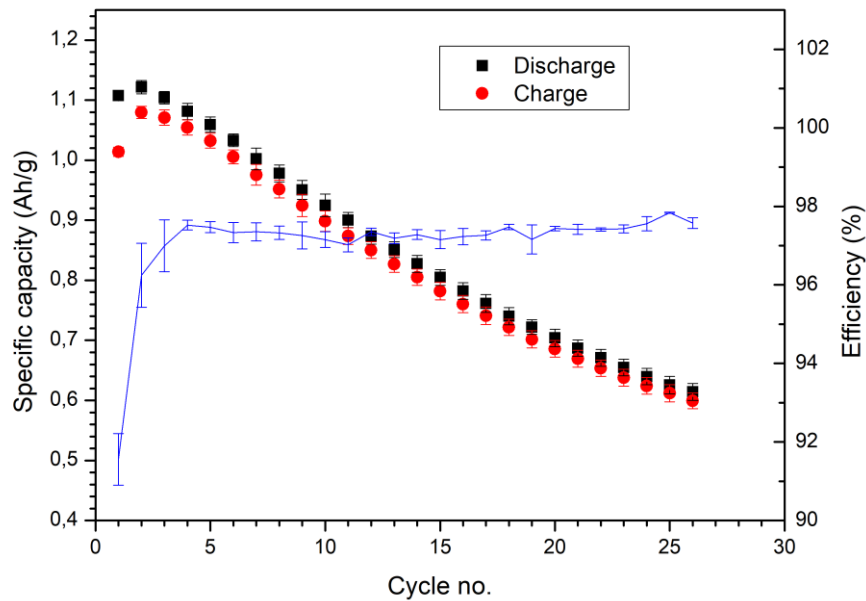


Figure 20: Cycling stability of the Gen-1 electrodes cycled using CCCV procedure.

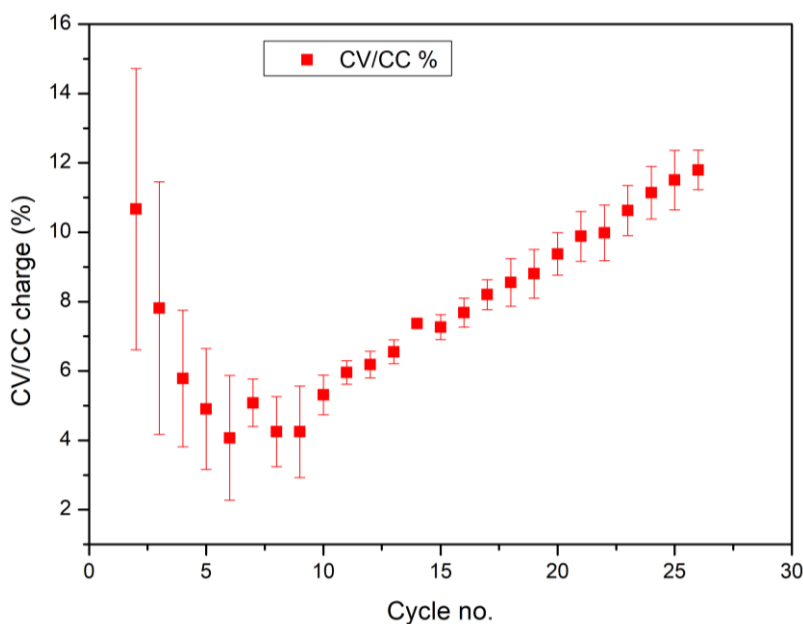


Figure 21: CV to CC ratio during each cycle.

9. ELECTROLYTE TRANSFERENCE NUMBER

The transference/transport number is a dimensionless parameter which informs about the contribution of the particular charged species present in the electrolyte to the overall charge transport across the cell. The determination of the Li ion transference number in the electrolyte was done using the Bruce and Vincent method.

The Bruce and Vincent method is commonly used for transference number determination in many electrolytes. An example of application in Li ion containing electrolytes was presented in (Zugmann, et al., 2011).

The experiment was done using Electrochemical Impedance Spectroscopy (EIS) and potentiostatic polarization measurement. The EIS measurement was done at a 100kHz-1Hz frequency range and 5 mV potential amplitude in a 2-electrode system. The potentiostatic polarization of +10 mV was performed for 1 hour (3600 sec). Both experiments were done at a Solatron 1260 device. The final value of the transference number was calculated using the following equation:

$$t_{Li} = \frac{I_{SS}(V - I_0 R_0)}{I_0(V - I_{SS} R_{SS})}$$

Where I_{SS} and R_{SS} are the steady state current and cell resistance at steady state, I_0 and R_0 are the initial current and cell resistance in the initial current, and V is the applied potential.

The measured EIS spectra was simulated using a $R_e(R_1CPE1)(R_2CPE2)$ equivalent circuit, with $R_1 + R_2$ equal to R_0 or R_{SS} , respectively. R_e is the electrolyte resistance. Because of electrode roughness and other surface phenomena, the electrode resistances are combined with constant phase elements. The simulation is very well fitted to the measured data.

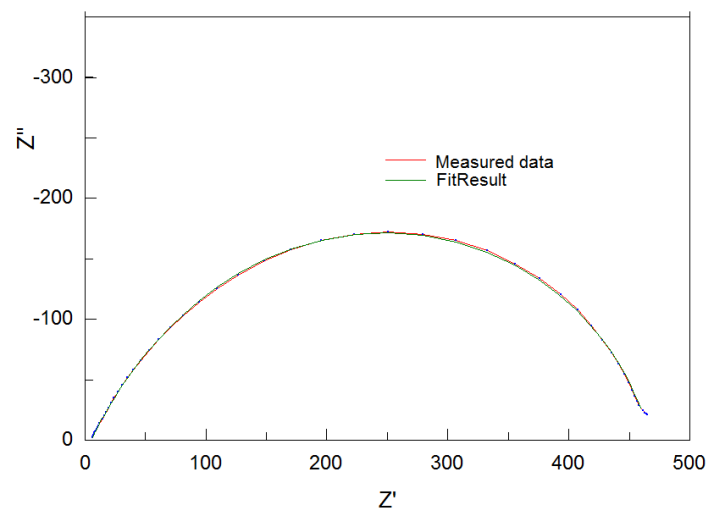


Figure 22: EIS data and fitted curve used for I_{ss} parameter determination.

R_{SS} and R_0 estimated from the EIS spectra are 463.8 Ohm and 450.3 Ohm respectively.

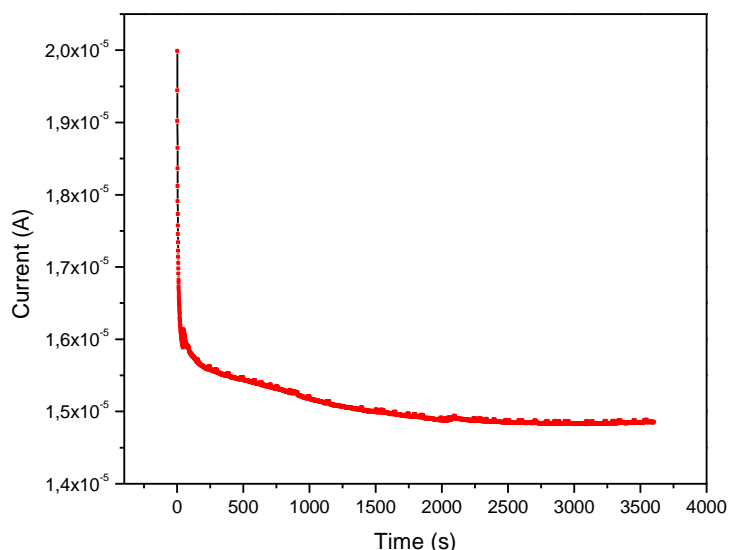


Figure 23: Current vs. Time in potentiostatic experiment.

I_{SS} and I_0 obtained from the potentiostatic experiment are $1.999E-5$ (A) and $1.483E-5$ (A) respectively.

The Transference number obtained from the equation is $t_+=0.248$.

It is in good agreement with the values 0.24 and 0.28 obtained for 1M LiPF₆ in EC/DEC (Zugmann, et al., 2011). The values obtained for different Li salt concentration cannot be compared due to the concentration dependence of the transference number.

10. EXCHANGE CURRENT DENSITY – GEN 1

The exchange current density was measured using method 1 equation 11 from (Ecker, et al., 2015). Following assumptions were made:

CT coefficient = $\alpha = 0.5$

The electrode surface contacted with the electrolyte was calculated using equation 9 from the reference above, assuming 9% of inactive part (2% carbon black and 7 % binder). A porosity factor of 0.3 was used for the calculations.

Calculated electrode surface (ECSA) 20.8 cm^2 – geometric SA= 0.636 cm^2

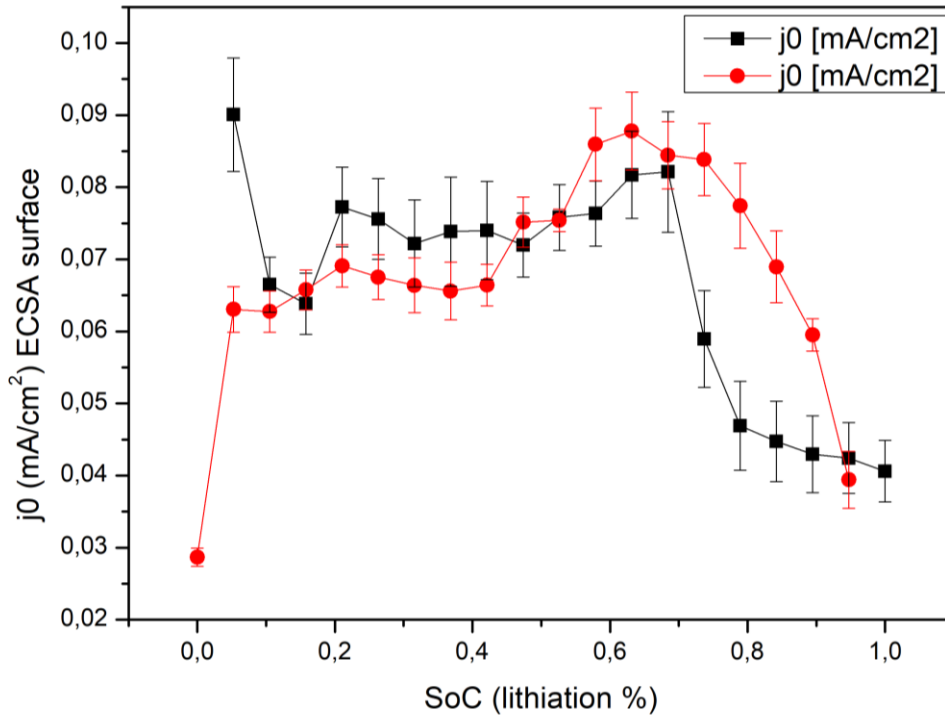


Figure 24: Exchange current density (Per ECSA surface) in a function of lithiation degree. Black -lithiation, red-delithiation

11. ENTROPIC COEFFICIENT – GEN 1

The entropic coefficient was measured in an asymmetric, isothermal cell with lithium counter electrode. At a specific SoC, the temperature was stabilized at 20°C for a minimum of 2 hours, and then increased to 35°C during a 4-hour period. At each temperature, the voltage change between the Gen 1 and Lithium electrode was recorded. The temperature stabilization time was longer than necessary for the equilibration of the OCV.

The cell was then discharged for approx. 6% of the maximum capacity and the temperature measurements were repeated.

The obtained OCV/K change was corrected by the lithium metal entropic coefficient according to (Swiderska-Mocek, Rudnicka, & Lewandowski, 2019) and (Bazinski & Wang, 2014).

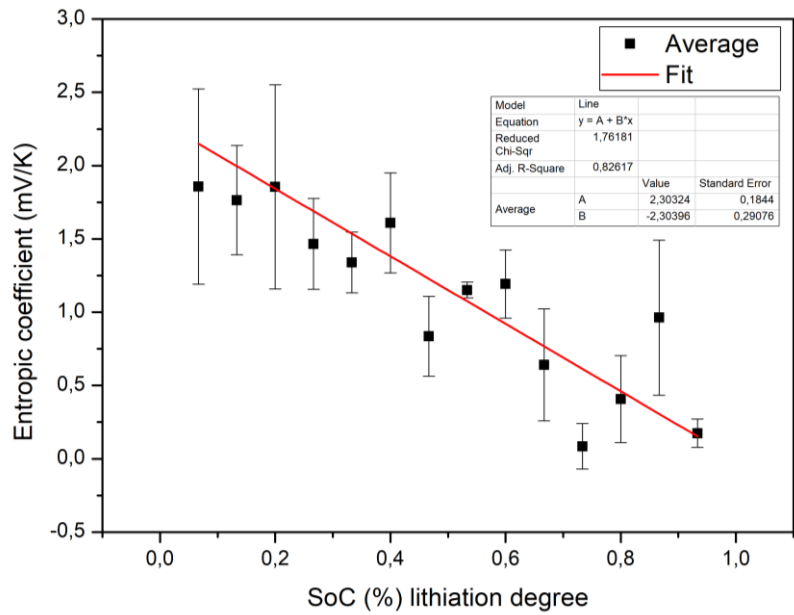


Figure 25: Gen-1 electrodes entropic coefficient.

12. ACTIVATION ENERGY – GEN 1

The activation energy was calculated based on the EIS data recorded at different temperatures using the calculations presented in (Yang, Yan, Wu, Lu, & Zeng, 2017) and (Okubo, Tanaka, Zhou, Kudo, & Honma, 2009). The diffusion coefficient was calculated from the low frequency EIS data from the $\text{mod}(Z)$ vs $\sqrt{\omega}$ slope. The change in the diffusion coefficient logarithm is related to $(-E_a/k)$ factor, there k is the Boltzman constant.

The calculated activation energy $E_a = 0.41 \pm 0.02 \text{ eV}$

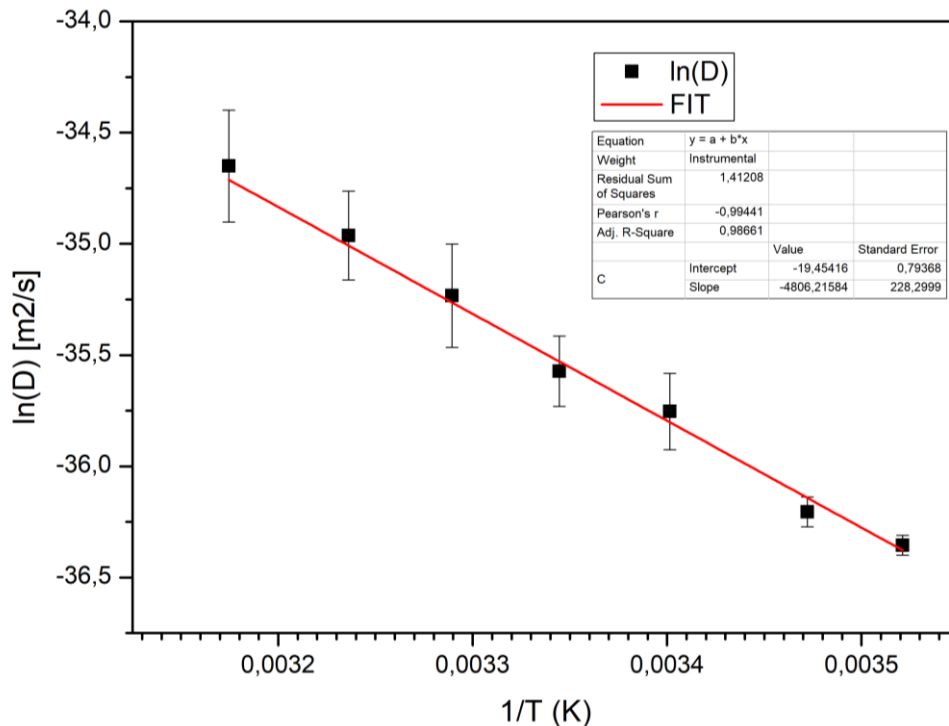


Figure 26: Logarithm of the diffusion coefficient at different temperatures from 10°C to 42°C.

Literature

- Bazinski, S. J., & Wang, X. (2014). The Influence of Cell Temperature on the Entropic Coefficient of a Lithium Iron Phosphate (LFP) Pouch Cell. *Journal of The Electrochemical Society*, 161(1), pp. 168-175.
- Ecker, M., Tran, T. K., Dechent, P., Käbitz, S., Warnecke, A., & Sauer, D. U. (2015). Parameterization of a Physico-Chemical Model of a Lithium-Ion Battery: I. Determination of Parameters. *Journal of The Electrochemical Society*, 162(9), pp. 1836-1848.
- Ehrl, A., Landesfeind, J., Wall, W. A., & Gasteiger, H. A. (2017). Determination of Transport Parameters in Liquid Binary Lithium Ion Battery Electrolytes. *Journal of The Electrochemical Society*, 164(4), pp. 826-838.
- France-Lanord, A., & Grossman, J. C. (2019). Correlations from Ion Pairing and the Nernst-Einstein Equation. *Physical Review Letters*, 122(13), p. 136001.
- Greenwood, N. N., & Earnshaw, A. (1997). *Chemistry of the Elements* (2 ed.).
- Iermakova, D. I., Dugas, R., Palacín, M. R., & Ponrouch, A. (2015). On the Comparative Stability of Li and Na Metal Anode Interfaces in Conventional Alkyl Carbonate Electrolytes. *Journal of The Electrochemical Society*, 162(13), pp. A7060-A7066.
- Keech, P. G., Chartrand, M. M., & Bunce, N. J. (2002). Oxidation of simple indoles at a platinum anode. *Journal of Electroanalytical Chemistry*, 534(1), pp. 75-78.
- Kim, H., Chou, C.-Y., Ekerdt, J. G., & Hwang, G. S. (2011). Structure and Properties of Li-Si Alloys: A First-Principles Study. *The Journal of Physical Chemistry C*, 115, pp. 2514-2521.
- Latifatu, M., Bon, C. Y., Lee, K. S., Hamenu, L., Kim, Y. I., Lee, Y. J., . . . Ko, J. M. (2018). Structural Effect of Conductive Carbons on the Adhesion and Electrochemical Behavior of $\text{LiNi}_{0.4}\text{Mn}_{0.4}\text{Co}_{0.2}\text{O}_2$ Cathode for Lithium Ion Batteries. *Journal of the Electrochemical Science and Technology*, 9(4), pp. 330-338.
- Masaya, I. (2002). Estimation of the atomic density of amorphous carbon using ion implantation, SIMS and RBS. *Surface & Coatings Technology*, 158, pp. 377-381.
- McCulloch, D. G., McKenzie, D. R., & Goringe, C. M. (2000). Ab initio simulations of the structure of amorphous carbon. *Physical Review B*, 61(3), pp. 2349-2355.
- Nickol, A., Schied, T., Heubner, C., Schneider, M., Michaelis, A., Bobeth, M., & Cuniberti, G. (2020). GITT Analysis of Lithium Insertion Cathodes for Determining the Lithium Diffusion Coefficient at Low Temperature: Challenges and Pitfalls. *Journal of The Electrochemical Society*.
- Nysted, V. S. (2020). The galvanostatic intermittent titration technique for silicon-based li-ion battery anodes: theory and experimental validation.
- Okubo, M., Tanaka, Y., Zhou, H., Kudo, T., & Honma, I. (2009). Determination of Activation Energy for Li Ion Diffusion in Electrodes. *The Journal of Physical Chemistry B*, 113(9), pp. 2840-2847.
- Pearson, G. L., & Bardeen, J. (1949). Electrical Properties of Pure Silicon and Silicon Alloys Containing Boron and Phosphorus. *Physics Review*, 75(5), pp. 865-883.
- Ratynski, M., Hamankiewicz, B., Buchberger, D. A., Boczar, M., Krajewski, M., & Czerwinski, A. (2020). A New Technique for In Situ Determination of the Active Surface Area Changes of Li-Ion Battery Electrodes. *Batteries & Supercaps*, 3(10), pp. 1028-1039.
- Roy, B. N., & Wright, T. (1996). Electrical Conductivity in Polycrystalline Copper Oxide Thin Films. *Crystal Research & Technology*, 31(8), pp. 1039-1044.

- Schwan, J., Ulrich, S., Theel, T., Roth, H., & Ehrhardt, H. (1997). Stress-induced formation of high-density amorphous carbon thin films. *Journal of Applied Physics*, 82, pp. 6024-6030.
- Swiderska-Mocek, A., Rudnicka, E., & Lewandowski, A. (2019). Temperature coefficients of Li-ion battery single electrode potentials and related entropy changes – revisited. *Physical Chemistry Chemical Physics*, 21(4), pp. 2115-2120.
- Xia, L., Lee, S., Jiang, Y., Xia, Y., Chen, G. Z., & Liu, Z. (2017). Fluorinated Electrolytes for Li-Ion Batteries: The Lithium Difluoro(oxalato)borate Additive for Stabilizing the Solid Electrolyte Interphase. *ACS Omega*, 2(12), pp. 8741-8750.
- Yang, S., Yan, B., Wu, J., Lu, L., & Zeng, K. (2017). Temperature-Dependent Lithium-Ion Diffusion and Activation Energy of $\text{Li}_{1.2}\text{Co}_{0.13}\text{Ni}_{0.13}\text{Mn}_{0.54}\text{O}_2$ Thin-Film Cathode at Nanoscale by Using Electrochemical Strain Microscopy. *ACS Applied Materials & Interfaces*, 9(16), pp. 13999-14005.
- Zugmann, S., Fleischmann, M., Amereller, M., Gschwind, R. M., Wiemhöfer, H. D., & Gores, H. J. (2011). Measurement of transference numbers for lithium ion electrolytes via four different methods, a comparative study. *Electrochimica Acta*, 56(11), pp. 3926-3933.